This is a repository copy of *Fluid effects on the dilatancy of two-phase gravity-driven granular flows*.

White Rose Research Online URL for this paper:
https://eprints.whiterose.ac.uk/id/eprint/232359/

Version: Accepted Version

Article:

Zhao, Y. orcid.org/0000-0002-5594-598X, Bowman, E.T. orcid.org/0000-0001-7868-6688, Zhou, G.G.D. orcid.org/0000-0001-9014-2931 et al. (3 more authors) (2025) Fluid effects on the dilatancy of two-phase gravity-driven granular flows. Physics of Fluids, 37 (9). 093329. ISSN: 1070-6631

https://doi.org/10.1063/5.0291548

© 2025 The Authors. Except as otherwise noted, this author-accepted version of a journal article published in Physics of Fluid is made available via the University of Sheffield Research Publications and Copyright Policy under the terms of the Creative Commons Attribution 4.0 International License (CC-BY 4.0), which permits unrestricted use, distribution and reproduction in any medium, provided the original work is properly cited. To view a copy of this licence, visit http://creativecommons.org/licenses/by/4.0/

Reuse

This article is distributed under the terms of the Creative Commons Attribution (CC BY) licence. This licence allows you to distribute, remix, tweak, and build upon the work, even commercially, as long as you credit the authors for the original work. More information and the full terms of the licence here: https://creativecommons.org/licenses/

Takedown

If you consider content in White Rose Research Online to be in breach of UK law, please notify us by emailing eprints@whiterose.ac.uk including the URL of the record and the reason for the withdrawal request.

eprints@whiterose.ac.uk
https://eprints.whiterose.ac.uk/

ACCEPTED MANUSCRIPT

Physics of Fluids

AIP Publishing

This is the author's peer reviewed, accepted manuscript. However, the online version of record will be different from this version once it has been copyedited and typeset.

PLEASE CITE THIS ARTICLE AS DOI: 10.1063/5.0291548

Fluid Effects on the Dilatancy of Two-phase Gravity-driven Granular Flows

Yuting Zhao[a], Elisabeth T. Bowman[b], Gordon G.D. Zhou[a, c, d, *], Kahlil F.E. Cui[a], Yunxu XIE[a, c], Xueqiang Lu[a]

[a] Key Laboratory of Mountain Hazards and Engineering Resiliences / Institute of Mountain Hazards and Environment, Chinese Academy of Sciences, Chengdu 610000, China
[b] School of Mechanical, Aerospace and Civil Engineering, University of Shefeld, Shefeld S1 3JD, UK
[c] University of Chinese Academy of Sciences, Beijing 100000, China
[d] China-Pakistan Joint Research Center on Earth Sciences, CAS-HEC, Islamabad, Pakistan

Corresponding author: Gordon G.D. Zhou
Email address: gordon@imde.ac.cn

Key words: Granular flow; Multiphase flow; Flume experiment; Volume fraction; Two-phase flow model

ABSTRACT

Volume fraction of solid grains plays a critical role in determining the dynamics of granular flows. The evolution of volume fraction is governed by flow dilatancy depending on the rheological behaviour of solid-fluid mixtures and hence the pore fluid effects, which are dominated by apparent cohesion and viscous drag in unsaturated and saturated flows, respectively. Prevailing approaches for predicting volume fraction in wet granular flows using two-phase flow models have been proven valid for submerged granular flows or suspensions that conform to visco-inertial rheology. However, for unsaturated granular flows, widely accepted methods for volume fraction modelling remain lacking, due to the cohesive interaction mechanisms not yet being fully described. In this study, we conducted small-scale flume experiments using uniform pseudo-spherical ceramic beads, with initial water content progressively varied from dry to oversaturated states. The dynamics of the experimental flows were captured by sensor measurements and image processing techniques, with solid volume fraction evolution obtained by Particle Tracking Velocimetry (PTV). We incorporated our experimental data into the $\mu(K)$ (visco-inertial) and $\mu(I_m)$ (extended inertial) rheological frameworks constructed for two-phase flows and then contrasted the fitting performance of the two corresponding volume fraction scaling models, $\Phi(K)$ and $\Phi(I_m)$, through error analysis. We demonstrate here for the first time the excellent validity of $\Phi(I_m)$ scaling for both unsaturated and saturated granular flows in which the dominated fluid effect ranges from apparent cohesion to viscous shear; by contrast, $\Phi(K)$ scaling shows significantly better applicability to saturated granular flows than to unsaturated flows.

Physics of Fluids ACCEPTED MANUSCRIPT
AIP Publishing
This is the author's peer reviewed, accepted manuscript. However, the online version of record will be different from this version once it has been copyedited and typeset.
PLEASE CITE THIS ARTICLE AS DOI: 10.1063/5.0291548

I. INTRODUCTION

Granular flows, movements of collections of solid particles, are prevalent in both industrial processes and natural geophysical hazards[1]. The dynamics of granular flows are determined by many factors, a crucial one of which is solid volume fraction, denoted by Φ, defined as the ratio of the volume occupied by solid grains to the total volume of the assembly[2] . Typical values of volume fraction may range from 0.55 to 0.64 for uniform spherical particles[3], and from 0.5 to 0.8 for natural debris flows[4]. Volume fraction controls the rheological responses of granular media, especially the free-surface flows that are highly relevant to geophysical phenomena[5]. A higher volume fraction generally leads to frictional shear dominated by enduring intergranular contacts, whereas a lower volume fraction relates more to inertial motions by transient collisions[6]; these different momentum transfer mechanisms govern the flow regimes from a dilute saltating "gas" state, to a dense but flowing "liquid" state, to a quasi-static "solid" state, coupled with an evolution of volume fraction from low to high[7]. Thus, the evolution of solid volume fraction is of great significance for capturing the granular flow behaviour.

The evolution of volume fraction is strongly connected with the shear-induced deformation of flow material. Based on the critical state theory[8, 9], a dilating granular flow becomes more fluidised and its volume fraction decreases, while a contracting flow tends to be more stabilised when its volume fraction increases[10, 11]. These responses under shear are vital to geophysical flow processes from initiation to deposition[12-15], and are dependent on material composition (e.g. grain shape and size distribution), initial packing density (i.e. dense or loose packing), stress states (e.g. normal and shear stress) and shear patterns (i.e. shear rate)[16-20]. Modern theoretical frameworks describing dry granular flows often adopt the inertial number, I, to summarise the dependence of volume fraction on shear rate and normal stress, $\Phi(I)$, as a supplementary product of the well-known $\mu(I)$ rheology[21-23]. Inertial number is defined as the ratio of grain inertia to confining stress[24], making it physically equivalent to the classic Savage number which is the ratio of collisional stress to frictional stress[4]. For dense dry granular flows in inertial to quasi-static regime, volume fraction increases when flow dilates at high inertial number and decreases when flow contracts at low inertial number[25]. In general, the $\Phi(I)$ relationship sets up a fundamental framework for modelling volume fraction variations with flow motion.

The existence of viscous pore fluid in wet granular flows, which are more common in a geophysical context, introduces extra controlling factors to the evolution of the volume fraction. If the solid particles are immersed in pore fluid, the dominated momentum transfer mechanism during solid-fluid interactions can be different. For immersed granular flows or suspensions, viscous fluid shear *within the interstitial spaces can lubricate the solid contacts and hence contribute to the flow dilation*[26-28]*. This viscous effect* on rheological response can be characterised by a dimensionless viscous number, J, which is defined by the ratio between viscous shear stress and confining stress[29]; volume fraction can then be presented by $\Phi(J)$ following a similar framework as in dry cases[30, 31]. Later, the inertial number and viscous number were integrated into a combined dimensionless visco-inertial number, K, allowing $\Phi(K)$ to model the volume fraction evolution for flows across different regimes from dominated by solid inertia to dominated by fluid viscous drag[32]. On the other hand, when pore fluids are unable to be expelled from the interstitial spaces within granular skeleton, variation in volume fraction cannot occur without feedback from pore fluid pressure which governs the solid-fluid interactions: dilation of the granular medium can result in a decrease in pore pressure by sucking pore fluid into the voids, hence

AIP Publishing Physics of Fluids ACCEPTED MANUSCRIPT
This is the author's peer reviewed, accepted manuscript. However, the online version of record will be different from this version once it has been copyedited and typeset.
PLEASE CITE THIS ARTICLE AS DOI: 10.1063/5.0291548

strengthening intergranular effective stresses and hindering a further increase in volume fraction; conversely, contraction of the mixture can increase pore pressure, reducing effective stresses or even liquefying the solids, thereby preventing further reduction of the volume fraction[33]. This damping effect on the transient variations in volume fraction can be connected to the intrinsic permeability of the granular material through the ratio between the timescale of translational flow motion and that of pore pressure dissipation[34]. In short, the two major pore fluid influences on solid grains in gravity-driven granular flows – viscous shear due to solid-fluid relative movement and pore pressure that resists the grain rearrangement[35] – play crucial roles in volume fraction evolution and have been widely considered in advanced granular flow models[36-38].

Unlike fully dry or saturated scenarios, unsaturated or partially saturated granular flows have been little studied, despite their ubiquity in the forms of fluidised bed, rainfall-induced landslides, segregated debris flows, etc[39]. A clear fact is that pore water insufficient to fill up interstitial spaces tends to attach to the surface of solid particles, forming capillary bridges between solid particles and resulting in macroscopic cohesion and enhanced shear strength[40, 41]; this is also known as matric suction in unsaturated soil mechanics[42, 43]. In such cases, the energy dissipation between solid and fluid phases is dominated by this suction or apparent cohesion, rather than by viscous fluid drag, hence pore fluid produces a "cohesive" instead of "viscous" effect on the grain-fluid mixture. Experiments have shown that unsaturated flows exhibit higher shear resistance and lower velocity or mobility[44, 45]. Consequently, dilation is inhibited in flows with greater cohesion or suction effects and thus volume fraction should stay relatively high. However, some evidence also indicates that volume fraction may decrease with apparent cohesion in unsaturated granular media under steady shear or vibration[46, 47]. This contradiction demonstrates that fundamental mechanisms of unsaturated granular flows remain poorly understood and the estimation of volume fraction in flows with low water content remain doubtful. In recent research, Vo, et al.[48] has incorporated the effects of apparent cohesion in unsaturated granular flows into an extended generalised inertial number, I_m, based on theoretical derivations and numerical simulation, leading to the development of a rheological framework that integrates various solid and fluid stresses and allowing the evolution of volume fraction to be modelled through a scaling relationship $\Phi(I_m)$. However, this model has not yet been supported by empirical data, which has hindered deeper insights into the dynamics of unsaturated granular flows. The underlying reason is that studies focusing on unsaturated flows — especially well-controlled and well-defined experimental investigations — remain scarce at present.

This study presents a series of small-scale flume experiments conducted using wet uniform granular materials with variable water content, where the saturation condition ranging from nearly dry (0.01) to oversaturated (0.40). The investigation focuses on the evolution of solid volume fraction with water content and explores the underlying dynamic mechanisms. Sensor measurements include basal normal stress, basal pore water pressure, and flow depth. A high-speed camera was used to record the motion of the flows and to allow the extraction of velocity fields and solid volume fractions through image analyses techniques, specifically Particle Image Velocimetry (PIV) and Particle Tracking Velocimetry (PTV). Finally, experimental data were used to compare the performance of existing two-phase flow models for prediction of volume fraction, thereby providing the first experimental validation of the recently proposed $\mu(I_m)$ and $\Phi(I_m)$ models, which can account for both cohesive and viscous fluid effects.

II. METHODOLOGY

ACCEPTED MANUSCRIPT
Physics of Fluids
AIP Publishing
This is the author's peer reviewed, accepted manuscript. However, the online version of record will be different from this version once it has been copyedited and typeset.
PLEASE CITE THIS ARTICLE AS DOI: 10.1063/5.0291548

A. Experimental Setup

The inclined flume system used in the experiments, as illustrated in FIG. 1, consisted of a metal hopper with a volume for releasing source materials, a 1.4-meter-long and 0.1-meter-wide channel fixed at an inclination of 30 degrees, a horizontal runout channel connected to the flume end, and an integrated data acquisition system. The hopper was equipped with a pneumatically controlled trapdoor, triggered by a microswitch linked to the data acquisition system to synchronise material release at the onset of data collection. The base of the inclined flume was covered with a mechanically roughened aluminium plate to provide a mild roughness at the basal boundary of tested flows.

Measurements were concentrated near the flume end to allow the flow to develop as much as possible. Two sensor pairs, each consisting of a load cell and a pore pressure transducer (PPT), were installed 100 mm (referred to as "downstream") and 365 mm (as "upstream") away from the flume end to measure the basal normal stress and pore water pressure of the flow mass. An ultrasonic sensor was mounted above the flume, aligned with the midpoint of the line connecting the centres of the downstream sensor pair, to measure the flow depth. All sensors were connected to the data acquisition system operating at a sampling frequency of 36 kHz. A high-speed camera was positioned at the side of the flume, with its field of view covering the sensor-installed zone, capturing a sequence of high-speed images for each experimental flow at a frame rate of 3000 fps.

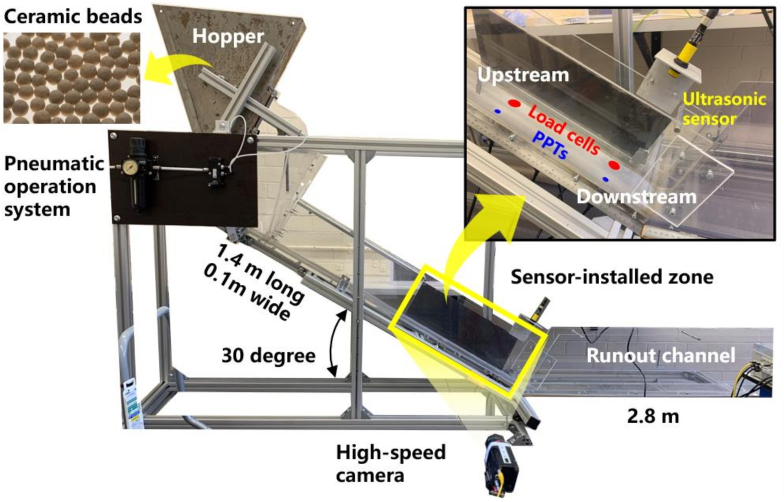

FIG. 1. Experimental setup.

B. Source Material

The solid material used in the experiments was Denstone® 2000 Support Media produced by Saint-Gobain Norpro. These pseudo-spherical ceramic particles with relatively rough surfaces are of an average particle diameter (δ) of 3.85 mm and a particle density of 2240 kg/m³. The average gravimetric water content (w) at saturation, which is measured by adding water to the static solid sample for each test until

ACCEPTED MANUSCRIPT
Physics of Fluids
AIP Publishing
This is the author's peer reviewed, accepted manuscript. However, the online version of record will be different from this version once it has been copyedited and typeset.
PLEASE CITE THIS ARTICLE AS DOI: 10.1063/5.0291548

water surface is level with the sample surface, was 0.256, corresponding to an average solid volume fraction (Φ) of 0.635and a material porosity (n) of 0.365. This granular material, as shown in the top left inset of FIG. 1, is well-suited for repeated experimental use due to its uniform particle size, chemical stability, and hardness, and has been applied to many studies[45, 49, 50]. The liquid fraction, characterised by water content, w, was selected as the test variable; seven values were adopted in the experiments: w = 0.00, 0.01, 0.10, 0.25, 0.30, 0.35, and 0.40, covering a spectrum of saturation condition from dry to oversaturated; on the other hand, the volume of solids was fixed at 2 litres throughout all the tests. For simplicity, each experiment is labelled by its water content, e.g. "w = 0.01".

At the beginning of each experiment, two litres of solid material were first poured into the sealed hopper, followed by the addition of water to achieve the target water content; leakage was effectively prevented by the waterproof trapdoor connected to the hopper opening. After thorough manual mixing, the prepared source material was released from the opened hopper into the inclined flume, forming a downslope unsteady granular flow and passing through the sensor-installed zone. The dynamic characteristics of the tested flow were then captured by the sensors and the high-speed camera. At the end, the flow entered the runout channel, where it came to rest and deposited.

C. Image Processing

High-speed images were analysed into the kinetics of tested flows via image processing methods. In our previous work[45], the flow velocity of experimental granular flows were obtained through Particle Image Velocimetry (PIV) analysis. However, since PIV only tracks images within a two-dimensional plane of the flow section, direct measurement of the solid volume fraction is unavailable. Particle Tracking Velocimetry (PTV), in contrast, adopts a Lagrangian framework wherein individual particles are identified and their trajectories tracked over time. This allows for the computation of volume fraction from the number of grains recognised in each frame. Thus, here PTV analysis is utilised to measure the evolution of volume fraction, giving a more comprehensive insight of the dynamics for all the tested flows. PTV analysis is done using PTVlab, an open-source MATLAB toolbox developed by Brevis, et al.[51] and later broadly used by many, e.g. Tauro, et al.[52] and Gomez, et al.[53]. This toolbox integrates a well-organised Graphical User Interface with advanced image processing and particle tracking algorithms to streamline PTV workflows.

PTV for dense granular flows, as previously described by Gollin, et al.[54], begins with centroid identification within the Region of Interest (in this study, a user-defined rectangular area covering the upstream or downstream load cell position), typically convolving a Gaussian reference mask with the image to generate initial centroid estimates, which are then refined by fitting an analytic function (such as a Gaussian) to each grain's intensity matrix for sub-pixel accuracy. Once precise centroid coordinates are obtained, particles are linked across successive frames to reconstruct trajectories. These trajectories yield instantaneous displacement vectors, enabling computation of velocity fields as well as higher-order statistics such as granular temperature and local solid volume fractions. A schematic illustration of the PTV procedure based on screenshots of running PTVlab is given in FIG. 2. For each experiment, through manual delimitation of the Region of Interest, PTV analyses were conducted at the upstream and downstream positions, respectively, to obtain the evolution of solid volume fraction in the tested flows during downslope motion. Note that in the screenshots, some grains on the top surface of the tested flow are in the camera view and are identified; this may lead to an overestimation of both the flow depth and

Physics of Fluids
ACCEPTED MANUSCRIPT
AIP Publishing
This is the author's peer reviewed, accepted manuscript. However, the online version of record will be different from this version once it has been copyedited and typeset.
PLEASE CITE THIS ARTICLE AS DOI: 10.1063/5.0291548

the particle count. Hence the ultrasonic sensor signals and the validated PIV data are used to determine the flow surface, above which the detected grains are excluded to ensure a more reliable particle count and therefore the volume fraction.

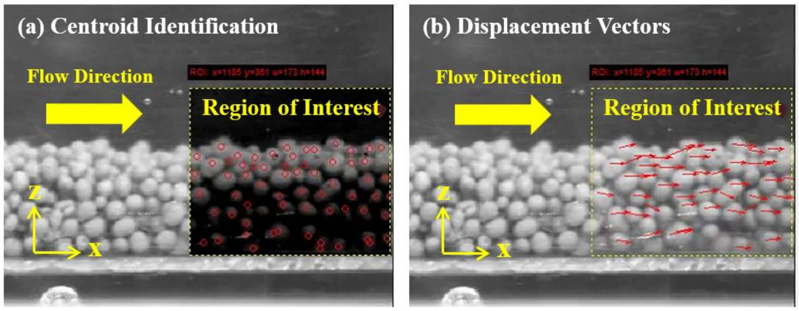

FIG. 2. PTV procedure of the tested flows: (a) centroid identification and (b) displacement vectors.

D. Dimensionless Characterisation

We first examine the dynamic similarity of our tests with other granular-flow experiments and natural geophysical flows through dimensional analysis[4, 35]. Two dimensionless parameters commonly used to characterize geophysical flow behaviours — the Savage number (N_{Sav}) and Bagnold number (N_{Bag}) — are employed to compare the present experimental results with other reported data. The Savage number is defined as the ratio of collisional stress arising from solid inertia to Coulomb frictional stress generated by enduring grain contacts, while the Bagnold number represents the ratio of collisional stress to the viscous shear stress of the interstitial fluid. The corresponding equations are given by[4, 12]:

$$N_{Sav} = \frac{\rho_s \Gamma^2 \delta^2}{\sigma'} \qquad (1)$$

$$N_{Bag} = \frac{\Phi}{1-\Phi} \frac{\rho_s \Gamma \delta^2}{\eta} \qquad (2)$$

where $\Gamma = \Delta v / h$ is bulk shear rate defined by the ratio of the difference between surface and slip velocity to the flow depth, σ' is basal effective normal stress, Φ is solid volume fraction and η is the pore fluid viscosity. The widely accepted thresholds are 0.1 for N_{Sav}[55] and 200 for N_{Bag}[56], above which the momentum exchange within the flow is dominated by grain inertia.

Error! Reference source not found. shows that the N_{Sav}–N_{Bag} values of our experiments align closely with those of large-scale experiments conducted by Taylor-Noonan, et al.[50] (using the same source material and similar setup) and Iverson[4]. Other small-scale experiments mostly show similar N_{Sav} but lower N_{Bag} values; this is likely due to the poorly-sorted solid materials adopted in these experiments with smaller mean particle sizes, making the solids more susceptible to viscous fluid drag. In contrast, few individual data points from experiments provided by de Haas, et al.[57] with similar N_{Bag} values to those in this study but higher N_{Sav} values are corresponded to cases

ACCEPTED MANUSCRIPT
Physics of Fluids
AIP Publishing
This is the author's peer reviewed, accepted manuscript. However, the online version of record will be different from this version once it has been copyedited and typeset.
PLEASE CITE THIS ARTICLE AS DOI: 10.1063/5.0291548

On the other hand, field data generally have greater N_{Bag} and cover a much broader range of N_{Sav} possibly due to their larger scales which extend particle settling times and substantially reduces interparticle effective stress. Despite not converging into a single master curve, all data points generally follow a power-law relationship of the form $N_{Bag} = AN_{Sav}^{B}$ where A and B are fitting constants. All datasets share the same slope (B) but differ in intercept (A): the field cases have higher A than our experiments, while the other experiments have lower A, shifting their trends vertically without changing the slope. In this respect, the present flume experiments are dynamically similar with previous experimental work and field observations.

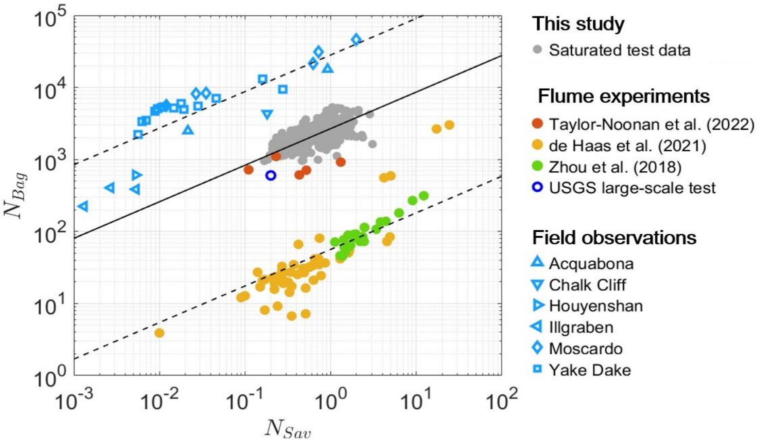

FIG. 3. Similarities between scaled experiments and field cases characterised by Savage number N_{Sav} and Bagnold number N_{Bag}. Data presented are from experimental work of Iverson[4], Taylor-Noonan, et al.[50], de Haas, et al.[57], Zhou, et al.[58], as well as field cases of Acquabona basin[59], Chalk Cliff[60, 61], Houyenshan ravine[62], Illgraben catchment[63-65], Moscardo Torrent[66] and Mountain Yake Dake[67-69].

It is important to note that dimensional analysis of field-scale flows often has to rely on rudimentary averaging of flow characteristics, e.g. using a single mean particle diameter to represent a wide grain size distribution or ignoring great difference in shear rate near the basal and free-surface boundaries. Experimental observations have demonstrated that dimensionless parameters in saturated granular flows notably vary with flow depth and characteristic grain size[70], raising questions about the physical significance of such analyses on field cases. However, more reliable relevance to large-scale flows can also be implied by direct comparisons of the granular-flow experiments presented in this and earlier studies[45] with those conducted in an over 8m-long flume at Queen's University, Canada*[50, 71]*, as they share highly similar experimental conditions in solid material, flume inclination, bed roughness, etc. Test results analysed by Zhao, et al.[45] and Taylor-Noonan, et al.[50] reveal consistent trends in depositional morphologies, flow behaviours, and normalised velocity profiles of granular flows across different scales. More straightforward comparisons can be found in Bowman, et al.[72, 73]. In conclusion, the small-scale experiments in this study not only demonstrate similarity in dimensionless groups with field cases but also exhibit cross-scale consistency in more specific dynamic characteristics, indicating their potential to represent the dynamics of large-scale geophysical flows to a reasonable extent.

AIP Publishing Physics of Fluids ACCEPTED MANUSCRIPT
This is the author's peer reviewed, accepted manuscript. However, the online version of record will be different from this version once it has been copyedited and typeset.
PLEASE CITE THIS ARTICLE AS DOI: 10.1063/5.0291548

III. RESULTS AND ANALYSES

A. Flow Profiles

Flow profiles of experiments in three different saturation states (i.e. dry, unsaturated and saturated) are displayed in FIG. 4, in which the tests w = 0.00, 0.10 and 0.40 are displayed in separate subfigures, and high-speed frames at the "leading edge", "flow front", "main body", and "flow tail" are presented. For each test, the "leading edge" is taken at the foremost part of the flow, "flow front" near the position where the flow depth reaches its visible peak, "main body" around the position after the peak flow depth where distinct changes in flow behaviour can be observed (for dry and unsaturated flows, this indicates further reduction in particle saltation, while for saturated flows, it corresponds to the emergence of a second surge), and "flow tail" at the position where the flow becomes thinner and more diffuse before it leaves from or comes to rest within the camera frame. Note that, although only three tests are given as examples here, other tests exhibit similar behaviours depending on in the unsaturated or saturated conditions.

All tested flows are led by dilute, saltating grains, indicating the formation of dry snouts in the experiments, with the fluid phase falling behind. For the dry flow, the front maintains a considerable degree of inertial motion, as evidenced by the surface-bouncing particles; the main body in the middle section is denser with most grains in sustained contacts, and shows a diluting tendency from upstream to downstream locations, before grains return to a more inertial state in the flow tail part. In contrast, for unsaturated flows with a small amount of pore water, grain saltation at the leading edge and flow head is significantly suppressed, and the flow maintains a relatively uniform but thinner depth throughout, until it stops and deposits on the slope as captured in the flow tail frame. For saturated flows, however, a thick and dense flow front immediately follows a moderately inertial leading edge and develops into a second surge characterised by a quick variation in flow depth, which then rapidly degrades into a thin and dispersive tail. Notably, the fluid surface can be observed outside the granular skeleton in the main body of the saturated flow (specifically, prior to the second surge) and persists through to flow tail, indicating a clear solid–fluid phase separation. In unsaturated flows, on the other hand, the pore fluid remains held within the granular body throughout the motion.

Based on these observable experimental phenomena, granular flows with identical solid volume but different water content exhibit markedly distinct behaviours, corresponding to the evolution of rheological characteristics: dry flows show the highest level of solid collisions, unsaturated flows experience enhanced resistance to shear motion, and saturated flows give the largest difference in flow depth between the front and tail, indicating that flow mass is more concentrated at the front.

ACCEPTED MANUSCRIPT

Physics of Fluids

AIP Publishing

This is the author's peer reviewed, accepted manuscript. However, the online version of record will be different from this version once it has been copyedited and typeset.

PLEASE CITE THIS ARTICLE AS DOI: 10.1063/5.0291548

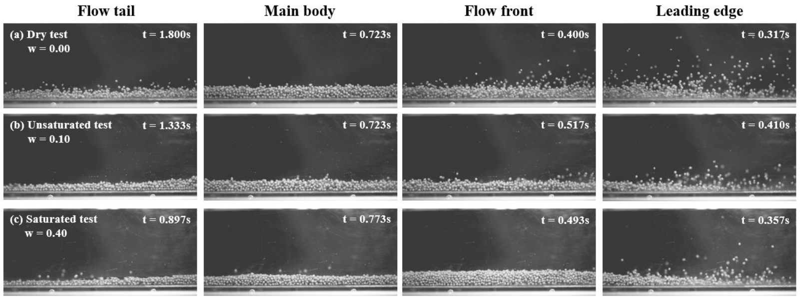

FIG. 4. Side-view flow profiles of (a) w = 0.00 dry test, (b) w = 0.10 unsaturated test and (c) w = 0.40 saturated test, with the leading edge, flow front, main body and flow tail displayed in four columns.

B. Volume Fractions

As variation in solid volume fraction in sheared granular flows is closely connected to dilative behaviours, evolution of volume fraction and flow depth should be considered together. The measured flow depth (h) normalised by grain size $(\delta = 3.85\ mm)$ and solid volume fraction (Φ) for all tested flows are shown in FIG. 5a and 4b, where data at upstream and downstream locations for unsaturated and saturated tests are demonstrated separately in four subplots; here, dry case is designated to the unsaturated subplot. For wet flows, upstream data are represented by red-toned curves and downstream data by blue-toned curves, whereas for the dry test the curves are depicted in grey and black, respectively; this colour scheme applies to all the data plots hereinafter. The x-axis uses normalised time, $(t - t_0)/(T - t_0)$, where t denotes time, t_0 is the time when flow depth reaches half the peak flow depth at the front and T the time when flow depth first falls to (or closest to) the same height near the tail, to provide a more intuitive comparison of the kinematics among tested flows with different durations. This approach excludes the saltating leading edges and the excessively shallow and slow-moving flow tail within the range $(t - t_0)/(T - t_0)\ \epsilon\ [0, 1]$. Note that this normalised time essentially represents the spatial distribution of dynamic characteristics within each tested flow, while the evolution with time is suggested in the difference between upstream and downstream.

As shown in FIG. 5a and 4b, although the difference varies with tests, the flows are consistently greater in both flow depth and volume fraction upstream than downstream, indicating that the unsteady granular flows become thinner and more dilute during downslope motion. This aligns with momentum conservation and commonly reported observations[74-76]. However, the spatial evolution of volume fraction does not always correspond to that of flow depth. Unsaturated flows tend to maintain a relatively stable volume fraction even as the flow depth gradually decreases after reaching its peak, while the volume fraction in saturated flows tend to decrease along with the flow depth reduction. Meanwhile, when contrasting different tests, the trend in flow depth for unsaturated flows shows a gradual decrease from the dry case to w = 0.10, with a slight increase as water content rises to w = 0.25; the trend in volume fraction, however, exhibits no significant differences except for w = 0.25 which is observably higher. For saturated flows with w = 0.30 – 0.40, visually apparent differences in flow depth also do not result in correspondingly prominent differences in volume fraction at the upstream location. Meanwhile at the downstream location, the volume fraction seems to subtly decrease with higher water content. This indicates that unsaturated flow bodies are less able to dilate due to the apparent cohesion, while saturated

ACCEPTED MANUSCRIPT
This is the author's peer reviewed, accepted manuscript. However, the online version of record will be different from this version once it has been copyedited and typeset.
PLEASE CITE THIS ARTICLE AS DOI: 10.1063/5.0291548

AIP Publishing

flows allow greater dilation as water content increases.

Tested flows exhibit an overall trend of increasing volume fraction levels with rising water content. As water content increases from 0.01 to 0.40, both upstream and downstream volume fractions around the peak flow depth increases gradually from approximately 0.4 to over 0.6. A noteworthy point is that, for all tested flows, volume fractions are consistently lower than the static value of 0.635, with very few exceptions. This agrees with the well-established fact that granular media must dilate to allow shear motion[77].

(a) Normalised Flow Depth Evolution against Normalised Time

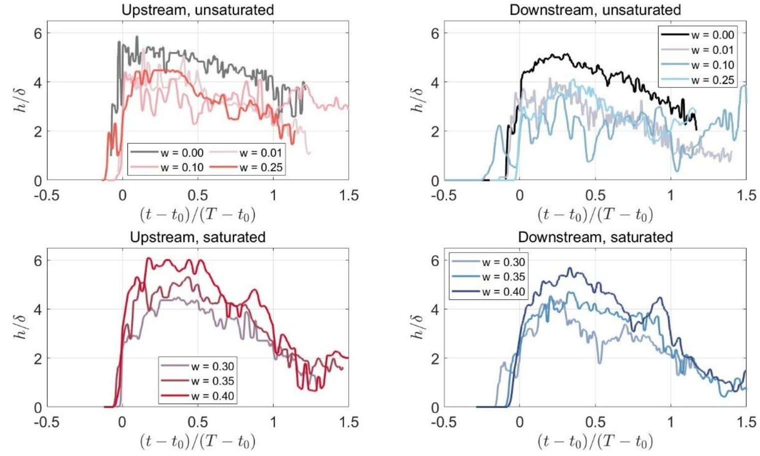

(b) Volume Fraction Evolution against Normalised Time

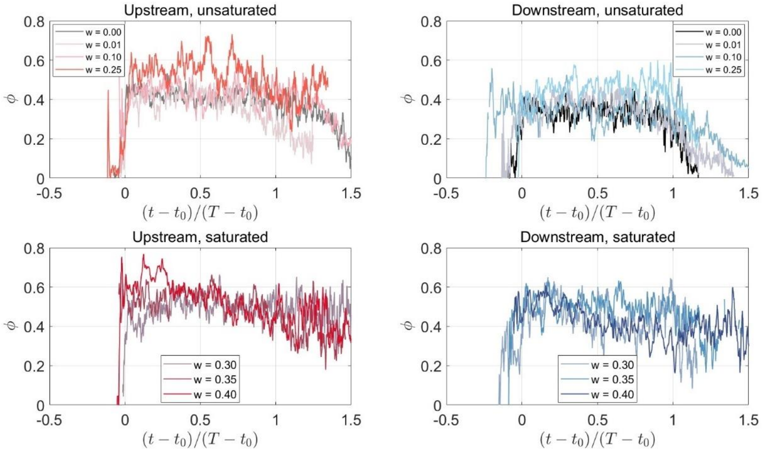

FIG. 5. Evolution of (a) normalised flow depth, h/δ, in mm and (b) volume fraction, Φ, against normalised time, $(t-t_0)/(T-t_0)$, where δ is grain size, t is time, t_0 and T are the moments when h first grows over and

Physics of Fluids ACCEPTED MANUSCRIPT
AIP Publishing
This is the author's peer reviewed, accepted manuscript. However, the online version of record will be different from this version once it has been copyedited and typeset.
PLEASE CITE THIS ARTICLE AS DOI: 10.1063/5.0291548

falls below half the peak flow depth, respectively.

C. Basal Pressures

In response to the clearly differentiated flow behaviours under different saturation conditions, pore pressures measured at the flume bed also exhibit a systematic evolution. FIG. 6a presents the development of basal pore pressures, p, for all tests against the normalised time, $(t-t_0)/(T-t_0)$, with data from upstream and downstream positions allocated in separate subplots. Data curves of unsaturated tests, i.e. water content w is smaller than its saturation value 0.256, are illustrated in dash lines, while those of saturated tests in solid lines. At both positions, pore pressure evolution with varying water content follows a consistent pattern. For the unsaturated experiments ranging from w = 0.00 to w = 0.10, the pore pressure is negative and decreases overall, indicating enhanced cohesion or suction effects. Note that for the dry test with no pore fluid, the negative pore pressure signals result from the passing dry granular body sucking part of the water out of the PPTs. As the water content increases to w = 0.25 close to the saturation threshold at static state, the pore pressure rises and approaches zero, reflecting a diminished cohesion. When water content further increases beyond saturation, positive pore pressure dominates throughout the flow, showing that cohesion effects gradually fade while buoyancy effects correspondingly take over. This gradual and continuous evolution of basal pore pressure with water content, and the inflection point of the trend, i.e. between w = 0.10 and w = 0.25, correspond well with the abrupt transitions observed in flow depth and solid volume fraction profiles given in FIG. 5.

Another clear trend is that pore pressure levels at the upstream position are systematically higher than those downstream, with decreasing positive values and increasing negative values during downslope motion. This is consistent with the decreased flow depth and increased solid volume fraction (FIG. 5): a reduction in flow depth decreases buoyancy, while local dilation promotes the growth of cohesion or suction. However, considering that, for the unsaturated flows with w = 0.00 – 0.10, the solid volume fraction changes only slightly whereas flow depth decreases markedly, the pore pressure differences between upstream and downstream are likely attributable primarily to differences in flow depth, even though the pore pressure within the flow body is dominated by negative values due to cohesive effects. This indicates that, regardless of the state of saturation, both buoyancy and cohesion coexist and compete within gravity-driven granular flows. In extreme cases (such as the unsaturated w = 0.10 or the saturated w = 0.40), cohesion or buoyancy dominates absolutely, rendering the other effects negligible. However, when the difference between the two is small, the weakening of buoyancy due to downslope motion can lead to the dominance of cohesion, potentially causing the flow to effectively exhibit unsaturated behaviours to some extent. For example, saturated flows with w = 0.30, where negative pore pressures occupy a larger space along the normalised time axis, volume fraction profiles also maintain a relatively stable level across the flow like unsaturated flows do (FIG. 5).

Given the fundamental role of pore pressure in regulating intergranular contacts, effective stress, σ', — defined as the difference between total normal stress, σ, and pore pressure, p, — is used to highlight the influence of pore pressure evolution on particle interactions. The evolution of the ratio between effective stress and total normal stress, σ'/σ, for all tests is shown in FIG. 6b, where unsaturated test data are still presented in dash lines and the normalised time, $(t-t_0)/(T-t_0)$, is confined within 0 – 1 to exclude the leading edge and flow tail parts where flow behaviours are more inconsistent. In

ACCEPTED MANUSCRIPT
Physics of Fluids
AIP Publishing
This is the author's peer reviewed, accepted manuscript. However, the online version of record will be different from this version once it has been copyedited and typeset.
PLEASE CITE THIS ARTICLE AS DOI: 10.1063/5.0291548

correspondence with the pore pressure evolution shown in FIG. 6a, as water content increases from zero, the ratio of effective stress to normal stress first exceeds 1 and continues to rise, reaching its highest level at w = 0.10, before gradually decreasing and dropping below 1 once saturation value is exceeded. This indicates that in unsaturated flows, intergranular frictional contacts are more robust than in dry granular flows, consistent with the cohesion effects, whereas in saturated flows, sustained particle contacts are reduced, allowing for greater inertial motion.

Moreover, for all wet granular flows, the ratio of effective stress relative to total normal stress is overall higher downstream than upstream. This suggests that even when solid volume fraction tends to decrease, as shown in FIG. 5, downslope motion still promotes an increase in the proportion of stress borne by the granular skeleton. This may imply that larger flow depths allow pore pressure to bear a greater proportion of intergranular contact stresses, echoing the scale effect of pore pressure proposed by Iverson[35].

(a) Pore Pressure against Normalised Time

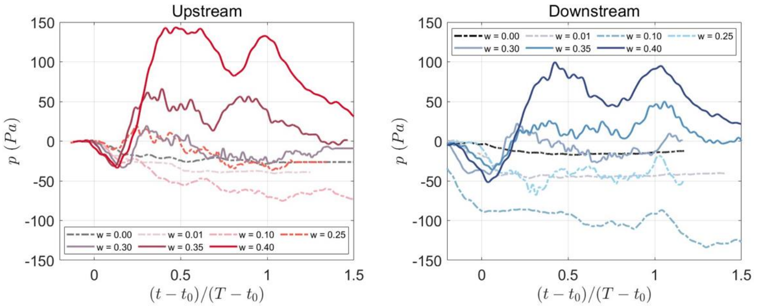

(b) Normalised Effective Stress against Normalised Time

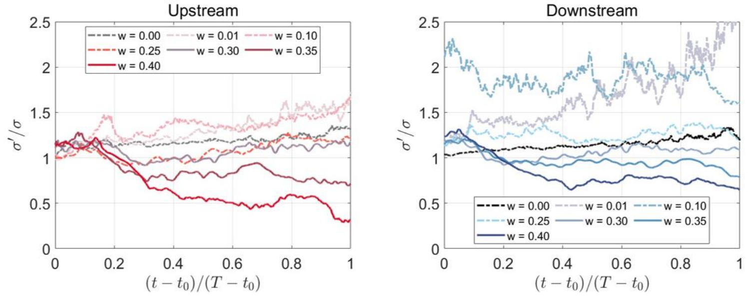

FIG. 6. Evolution of (a) basal pore pressure, p, and (b) the ratio of basal effective stress to total normal stress, σ'/σ, at upstream and downstream locations with water content. Data are plotted against normalised time, $(t-t_0)/(T-t_0)$, where t_0 and T are the moments when h first grows over and falls below half the peak flow depth, respectively.

D. Volume Fraction Modelling

To better understand the mechanisms by which increasing water content influences the evolution of solid

Physics of Fluids ACCEPTED MANUSCRIPT

AIP Publishing

This is the author's peer reviewed, accepted manuscript. However, the online version of record will be different from this version once it has been copyedited and typeset.

PLEASE CITE THIS ARTICLE AS DOI: 10.1063/5.0291548

volume fraction, it is essential to consider both the parameters affecting flow dilation and the contribution of pore fluid to the flow rheology. According to existing literature, key parameters controlling dilation behaviours include the initial volume fraction of the sample[18, 77], permeability of the flow material[33, 78], and flow regime showing the relative importance of grain inertia in momentum transfer[24, 79, 80]. In the present experiments, initial volume fraction and permeability of the source material are constant, hence the primary factors influencing the evolution of volume fraction in the tested flows are flow regime, characterised by different dimensionless numbers, depending on the rheological relationship.

For dense dry granular flows, the classic $\mu(I)$ rheology can be applied where the sole key parameter is the inertial number, I, defined as the ratio of gran inertial stress to confining pressure by[24]:

$$I = \sqrt{\frac{\rho_s}{\sigma'}}\Gamma\delta \quad (3)$$

in which $\rho_s = 2240\ kg/m^3$ is grain density, Γ is bulk shear rate and σ' is basal effective normal stress. Accordingly, the scaling function of solid volume fraction, $\Phi(I)$, is given by[21]:

$$\Phi(I) = \Phi_{max} + (\Phi_{max} - \Phi_{min})I \quad (4)$$

in which Φ_{max} and Φ_{min} are the achievable upper and lower limits of volume fraction under flow condition. Since both controlling parameters in Eq. 2 are of strict physical meanings, reasonable assumptions of their values can be determined. Here, $\Phi_{max} = 0.64$, which is the maximum random packing density of spheres and is also close to the static sample volume fraction of 0.635, and $\Phi_{min} = 0.3$, below which solid particles in tested flows tend to lose sustained contacts in the leading edge or flow tail, are taken, and the scaling function Eq. 2 is thus fixed.

To examine whether apparent cohesion generated by pore water in unsaturated flows indeed induce significant differences in rheological behaviours, data points for the dry test ($w = 0.00$) and two flows with the lowest water contents ($w = 0.01$ and 0.10) are distributed in the $\Phi - I$ coordinate space in FIG. 7, where data are selected at every 1% of the range from the maximum flow depth to $(t - t_0)/(T - t_0) = 1$ to prevent abrupt changes in flow regime. In addition, the root mean squared error (RMSE) of all data points from upstream and downstream positions relative to the scaling curve derived from Eq. 2, which is plotted as a solid black line, is also given in each subplot to more precisely evaluate the fitting performance of the rheological model; in most situations, an RMSE below 10% indicates a good level of agreement.

As shown in FIG. 7, only the dry flow with $w = 0.00$ exhibits good consistency with the scaling curve, with an RMSE around 7% which may be attributable to a few data points lying further from the curve. In contrast, data points for $w = 0.01$ and $w = 0.10$ deviate notably from the curve, with RMSE being 36% and 21% respectively, maintaining higher solid volume fractions at larger values of inertial number. This is consistent with the expectation that apparent cohesion formed within unsaturated flows enhances shear resistance and makes dilation more difficult, and indicates that even a very small amount of pore water added into a granular body can produce sufficient apparent cohesion to markedly influence the rheological response, invalidating the $\mu(I)$ and $\Phi(I)$ scaling relationships developed for inertial-frictional dense granular flows.

Physics of Fluids
AIP Publishing
ACCEPTED MANUSCRIPT
This is the author's peer reviewed, accepted manuscript. However, the online version of record will be different from this version once it has been copyedited and typeset.
PLEASE CITE THIS ARTICLE AS DOI: 10.1063/5.0291548

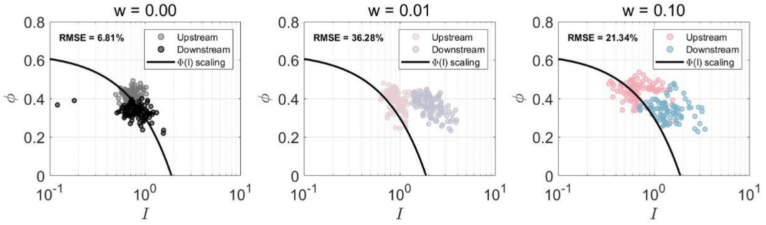

FIG. 7. Comparisons between $\Phi(I)$ scaling relationship and data from the tests w = 0.00, 0.01 and 0.10. Data are taken at every 1% of the range between where flow depth reaches its peak to where it reduces to its half near the flow tail for each test, while $\Phi(I)$ scaling is presented in black solid curves.

Before considering more complex cohesive effects, the well-established $\mu(K)$ rheology for immersed dense granular flows or suspensions, which is originally proposed by Trulsson, et al.[32] and later extended and applied by many (e.g. Tapia et al.[81], Amarsid et al.[82], Cui et al.[83], Xie et al.[84]), is first validated here. This rheology unifies the description of flow regimes spanning from dominated by solid inertia to dominated by viscous drag, through combining the inertial number (I) and viscous number (J) into a single dimensionless visco-inertial number, denoted by K, which characterises the additive effects of solid contacts and fluid viscous shear and is given by:

$$K = J + \alpha_i I^2 \tag{5}$$

in which J, defined as the ratio of fluid viscous stress to confining pressure, is calculated as [30]:

$$J = \frac{\eta \Gamma}{\sigma'} \tag{6}$$

where η is fluid dynamic viscosity, the value of which equals that of water as the contribution of air to viscous drag is assumed neglectable here. α_i is a constant depending on Stokes number calculated as:

$$St = \frac{\rho_s \delta^2 \Gamma}{\eta} = \frac{I^2}{J} \tag{7}$$

A boundary condition has been uncovered that the flow regime shifts from Newtonian viscous to Bagnoldian inertial when Stokes number $St = 1/\alpha_i$[32], hence a recommended value of α_i can be derived from the threshold of Stokes number. Although a definite threshold of Stokes number is not available, a reference value can be determined by adopting the Bagnold number, which is effectively equivalent to Stokes number but for dense granular assembly, with a suggested threshold of 200[4], yielding a reasonable value of $\alpha_i = 1/200 = 0.05$. Under this rheological framework, the scaling function of $\Phi(K)$, with a constant fitting coefficient α_K, is given as follows:

$$\Phi(K) = \Phi_{max}(1 - \alpha_K \sqrt{K}) \tag{8}$$

In FIG. 8, the $\Phi - K$ relationships for the wet experimental flows are plotted together with the $\Phi(K)$ scaling curve that achieves the best fit, where experimental data points are selected following the same approach as in FIG. 7, and the scaling curve is drawn in a solid blue line. In a corresponding supplementary figure, the local RMSE between data points and the scaling curve is displayed as yellow bar charts, with each bar height representing the RMSE of data points falling within the range between the K value at that bar's position and the value at the previous tick mark on the logarithmic axis. To

AIP Publishing
Physics of Fluids
ACCEPTED MANUSCRIPT
This is the author's peer reviewed, accepted manuscript. However, the online version of record will be different from this version once it has been copyedited and typeset.
PLEASE CITE THIS ARTICLE AS DOI: 10.1063/5.0291548

facilitate observation of the overall fitting performance, an averaged RMSE is also calculated and annotated on the bar chart, together with the corresponding α_K value yielding the best fit. As K only considers the viscous shear effects of fluid phase by its definition, the $\Phi(K)$ scaling curve is anticipated to show better agreement with saturated flows than unsaturated flows. Therefore, comparisons of the scaling curve with data points from all tests, from unsaturated tests only, and from saturated tests only, are respectively presented in the three subfigures of FIG. 8.

As expected, although $\Phi(K)$ scaling curve provides an overall satisfactory fit across all flows, larger errors can be observed in the unsaturated flows shown in FIG. 8b, while the best agreement is achieved with the saturated experimental data points in FIG. 8c. In subfigure 8a, the overall RMSE is 9.44%, slightly below 10%; the averaged RMSE for unsaturated flows reaches as high as 10.33%, whereas for saturated flows it sharply reduces to 6.61%, indicating that RMSE when comparing against all tests is pulled up by the larger deviations in the unsaturated tests.

Moreover, saturated flows maintain low local RMSE values across the entire spectrum of K, except for its lowest value, while unsaturated flows exhibit local RMSE values greater than 10% over more than a lower half of the K value range. The maximum local RMSE for all tested flows also appears in the region with the $K < 0.001$ values; this may result from insufficient data points magnifying the errors. However, data points of unsaturated tests stay mostly below the scaling curve where larger errors occur, showing again that unsaturated flows with notable cohesion or suction effects do not collapse well onto the $\Phi(K)$ scaling.

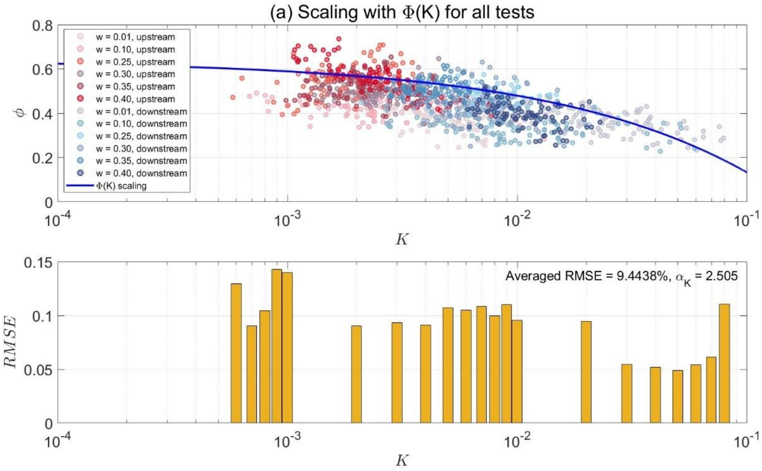
(a) Scaling with Φ(K) for all tests

ACCEPTED MANUSCRIPT
Physics of Fluids
AIP Publishing
This is the author's peer reviewed, accepted manuscript. However, the online version of record will be different from this version once it has been copyedited and typeset.
PLEASE CITE THIS ARTICLE AS DOI: 10.1063/5.0291548

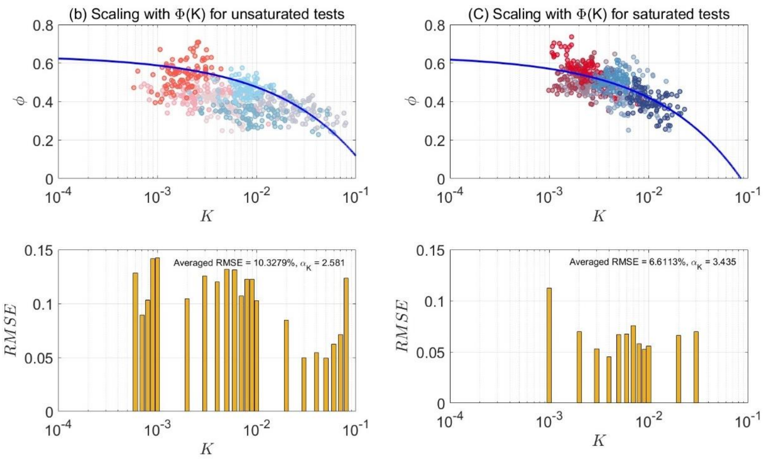

FIG. 8. The best fit between $\Phi(K)$ scaling relationship presented in blue solid curve and data from (a) all the wet tests, (b) unsaturated tests and (c) saturated tests, supported with bar charts of local root mean square errors (RMSE) of data points within each interval of K.

Due to the dominant effect of cohesion from the presence of limited pore fluid, unsaturated flows exhibit dilation behaviour that is obviously distinct from that of saturated flows. As shown in FIG. 8, within the $\Phi(K)$ framework, a broader range of K is required in unsaturated flows to achieve a decrease in solid volume fraction comparable to that of saturated flows, indicating a lower gradient or changing rate in solid volume fraction. This is consistent with the aforementioned observations that unsaturated flows tend to preserve more stable volume fractions compared to saturated flows (FIG. 5b), and to produce negative pore pressures that hold grains more tightly together (FIG. 6).

To explain the dilation behaviours and rheological characteristics of unsaturated flows, the dimensionless parameter used to describe the flow regime should account for the apparent cohesion or suction dominating the grain-fluid interactions, as well as the resultant enhanced effective stress. These factors contribute to the relatively low solid fraction gradients observed in unsaturated flows. Thus, an extended and modified inertial number, I_m, proposed by Vo, et al.[48], along with the corresponding scaling relationships with volume fraction, is employed here to describe the rheological evolution in all tested flows. The dimensionless number I_m, which potentially incorporates the effects of solid contacts, fluid cohesion and viscous shear, is expressed by:

$$I_m = I\sqrt{\frac{1+\beta/St}{1+\alpha\xi}} = \sqrt{\frac{\beta K}{1+\alpha\xi}} \tag{9}$$

where α is a material-dependent constant, β is a constant contributing to $I\sqrt{1+\beta/St}$ which is mathematically equivalent to $\beta\sqrt{K}$, hence $\beta = 1/\alpha_i = 200$, and ξ is cohesion index defined by the ratio of capillary stress to effective grain normal stress:

AIP Publishing Physics of Fluids ACCEPTED MANUSCRIPT
This is the author's peer reviewed, accepted manuscript. However, the online version of record will be different from this version once it has been copyedited and typeset.
PLEASE CITE THIS ARTICLE AS DOI: 10.1063/5.0291548

$$\xi = \frac{\gamma_s}{\sigma'\delta} \tag{10}$$

where γ_s is surface tension. Due to the apparent cohesion effects, the critical value of volume fraction, Φ_c, at quasi-static limit is no longer simply Φ_{max} but becomes dependent on ξ with the influence of a tuning constant b:

$$\Phi_c = \Phi_{max}(1 - b\xi) \tag{11}$$

With all these parameters given, the scaling relationship $\Phi(I_m)$ can be calculated with one additional fitting coefficient I_φ:

$$\Phi(I_m) = \frac{\Phi_c}{1 + I_m/I_\varphi} \tag{12}$$

As reflected in its formulation, the dimensionless parameter I_m is defined by incorporating effects of grain contacts and fluid viscous shear, with the additive contribution of apparent cohesion. Hence the $\Phi(I_m)$ scaling provides a generalised framework for more complex granular-flow regimes, encompassing fluid effects that transition from apparent cohesion to viscous drag.

Similar to FIG. 8, FIG. 9 evaluates the fitting performance of $\Phi(I_m)$ scaling against wet tested flows in three separate subfigures, dpending on the saturation condition. Each upper subplot in FIG. 9 presents a comparison between all experimental data points and the $\Phi(I_m)$ scaling curve, plotted as a red solid line, under the best-fit conditions; while in the lower subplot, local RMSE values within the I_m spectrum are shown as bar charts, with annotations indicating the average RMSE and the parameter values adopted in Eq. 7 – 10. Notably, experimental data in all the subfigures of FIG. 9 collapse neatly onto the scaling curves, showing an impressive level of agreement. Across the entire range of I_m values, almost all the local RMSE remain consistently below 10%, with the only exception being the maximum local RMSE for unsaturated flows (FIG. 9b) which slightly exceeds 10%. In all three cases, $\Phi(I_m)$ scaling give lower averaged RMSE than those appearing in FIG. 8; particularly, the averaged RMSE for unsaturated flows scaled with $\Phi(I_m)$ is only about 7.32%, showing a better fitting than $\Phi(K)$ which gives an averaged RMSE over 10%. This shows a clearly superior fitting accuracy of $\Phi(I_m)$ model than $\Phi(K)$ model for the two-phase granular flows, especially under the unsaturated condition.

Although originally derived through theoretical analysis and numerical simulations, the $\Phi(I_m)$ scaling relationship is successfully validated by the experimental data in this study, accurately capturing the evolution of solid volume fraction in granular flows ranging from highly unsaturated (w = 0.01) to oversaturated states (w = 0.40). This result confirms the feasibility and robustness of applying $\mu(I_m)$ and $\Phi(I_m)$ framework to granular flows exhibiting transitional rheological behaviours due to different dominated pore pressure effects.

AIP Publishing
Physics of Fluids
ACCEPTED MANUSCRIPT
This is the author's peer reviewed, accepted manuscript. However, the online version of record will be different from this version once it has been copyedited and typeset.
PLEASE CITE THIS ARTICLE AS DOI: 10.1063/5.0291548

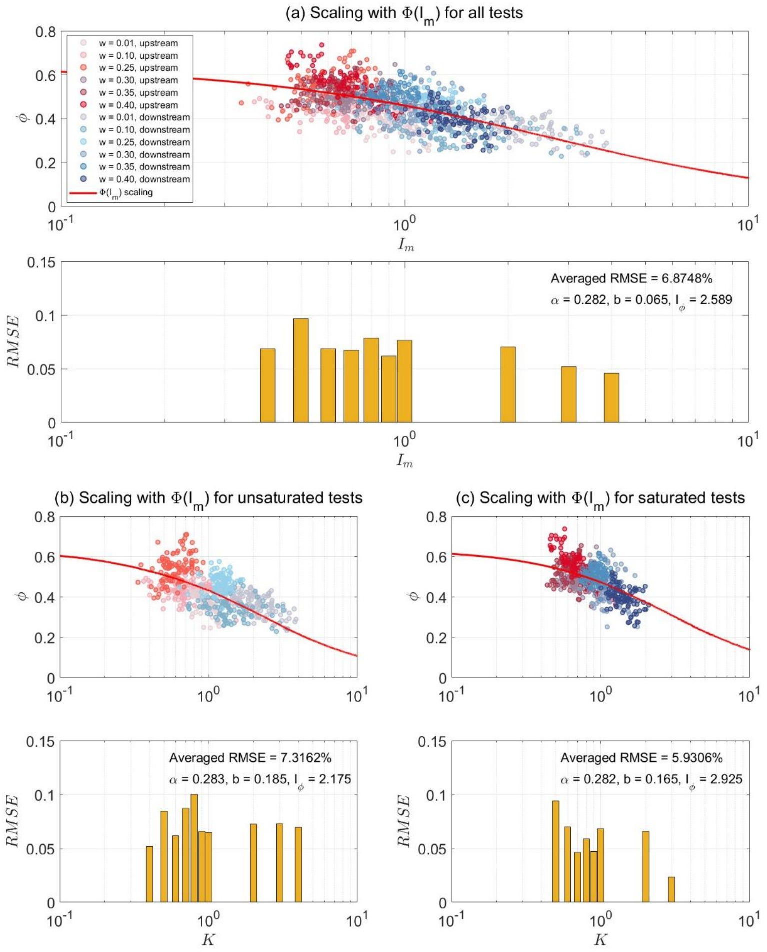

FIG. 9. The best fit between $\Phi(I_m)$ scaling relationship and data from (a) all the wet tests, (b) unsaturated tests and (c) saturated tests, supported with bar charts of local root mean square errors (RMSE) of data points within each interval of I_m.

Three volume fraction descriptions based on different rheological frameworks successfully capture the evolution of solid fraction in experiments under varying water content, and provide clear boundary conditions: $\Phi(I)$ scaling is valid only for dry granular flows without fluid, $\Phi(K)$ scaling is suitable for saturated granular flows but underperforms in the unsaturated condition, while $\Phi(I_m)$ scaling can be confidently utilised to describe unsaturated granular flows and also holds potential for application in saturated cases. This again highlights the influence of saturation degree on the rheological responses of granular flows, where a gradual transition of the dominated pore fluid effect from cohesion or suction that strengthens the frictional solid enduring contacts to buoyancy that facilitates inertial shear motion, echoing the transition of measured pore pressure from negative to positive.

AIP Publishing Physics of Fluids ACCEPTED MANUSCRIPT
This is the author's peer reviewed, accepted manuscript. However, the online version of record will be different from this version once it has been copyedited and typeset.
PLEASE CITE THIS ARTICLE AS DOI: 10.1063/5.0291548

IV. DISCUSSION

A. Effects of Regime Transition

In the two solid volume fraction scaling relations $\Phi(K)$ and $\Phi(I_m)$ presented earlier, the constant $\beta = 1/\alpha_i$ is set as a fixed value to enable a fair comparison of their scaling performance. However, the value of β does influence the ranges of K and I_m, thereby controlling the data point distribution and, to some extent, the scaling performance. An increase in β results in smaller calculated values of K but larger value of I_m which is proportional to $\sqrt{\beta K}$. Although $\beta = 1/\alpha_i$ has been found approximately equal to the transitional Stokes number (St) marking the flow regime shift from viscous to inertial dominance[32], the choice of this transitional St value does not have a definitive standard to date. Numerical simulations typically identify transitional St, referred to as β here for simplicity, between 1 – 2, e.g. $\beta = 1.0$ when volume fraction is below 0.57 – 0.59 by Ness and Sun[85], $\beta = 1.575$ by Trulsson, et al.[32] and $\beta = 2.0$ by Amarsid, et al.[82] from the best collapse of $\mu(K)$ and $\Phi(K)$. Rheological measurements in pressure-controlled experiments with varying fluid viscosity, on the other hand, has given a fixed $\beta = 10$ independent of volume fraction[81]. Whether obtained through numerical models or rheometer experiments, the transitional Stokes number is typically determined using uniform and steady granular flows or suspensions, which differ from the uniform but unsteady granular flows investigated in our flume experiments. Hence adopting the threshold Bagnold number commonly used in geophysical flows may be more appropriate. Nevertheless, the transition in flow regime defined under idealised conditions also has reference value as a comparison with scenarios closer to geophysical flows.

Using the experimentally measured value of transitional Stokes number $\beta = 10$, all our test data of wet granular flows are once again optimally fitted to both $\Phi(K)$ and $\Phi(I_m)$ scaling models, and the results are demonstrated in the two separate subplots in FIG. 10. Compared with FIG. 8 and FIG. 9 employing $\beta = 200$, the K values generally increased by an order of magnitude, and the averaged RMSE with the modelled volume fraction decreased by approximately 1%. In contrast, the I_m values, owing to the coefficient β appearing under a square root, exhibited almost no noticeable change, with the averaged RMSE increasing by only about 0.15% and still outperforming the $\Phi(K)$ scaling. These results indicate that the $\Phi(I_m)$ model demonstrates superior performance in terms of both fitting accuracy and robustness, regardless of the specific value chosen for the transitional Stokes number, suggesting a potential wide application range of the $\mu(I_m)$ and $\Phi(I_m)$ rheology.

AIP Publishing Physics of Fluids ACCEPTED MANUSCRIPT

This is the author's peer reviewed, accepted manuscript. However, the online version of record will be different from this version once it has been copyedited and typeset.
PLEASE CITE THIS ARTICLE AS DOI: 10.1063/5.0291548

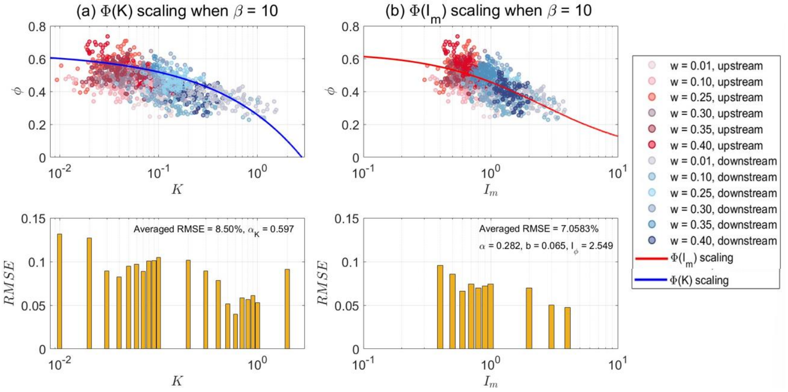

FIG. 10. Optimal (a) $\Phi(K)$ and $\Phi(I_m)$ scaling results when applying $\beta = 10$.

Considering that cohesion in unsaturated flows effectively reinforces enduring grain contacts and limits inertia-dominated flows, increasing the transitional Stokes number may be a "compromised" approach to somewhat incorporate cohesion effects into the $\Phi(K)$ model. The relationship between the inertial number, I, and the Stokes number, St, of the tested flows is shown in FIG. 11a, where black dashed line indicates a value of $I = \sqrt{0.1} = 0.316$, calculated based on the widely accepted threshold value of 0.1 of Savage number, which is a dimensionless number used in geophysical flows[4, 86] and is mathematically equivalent to the square of the inertial number; above this threshold, grain inertial stress overcomes Coulomb frictional stress. Although only few data points fall below this inertial number threshold, confirming that tested flows are inertia-dominated, it is possible to estimate a transitional Stokes number of approximately 900 corresponding to the inertial number threshold.

The optimal scaling between the $\Phi(K)$ model and the experimental data calculated with this increased transitional Stokes number value $\beta = 900$ is shown in FIG. 11b, including the accompanying RMSE bar chart. After increasing the β value, the $\Phi(K)$ scaling curve exhibits better agreement with the experimental data points, with an averaged RMSE that is reduced by nearly 2% compared to the case with $\beta = 200$ in FIG. 8, and the occurrences of local RMSE exceeding 10% are also improved. Combined with the results using $\beta = 10$ in FIG. 10, both larger and smaller values of β appear to allow better collapse of data points onto the $\Phi(K)$ curve, although the averaged RMSE remains higher than that of the $\Phi(I_m)$ scaling. This may be because the region with higher curvature in the middle section of the $\Phi(K)$ curve is partially avoided when data distribution range shifts left or right on the logarithmic axis through the adjustment of β. Therefore, whether the increase of coefficient β should be regarded as a workable consideration of cohesion effects or only as part of tuning needs further investigation.

ACCEPTED MANUSCRIPT
Physics of Fluids
AIP Publishing
This is the author's peer reviewed, accepted manuscript. However, the online version of record will be different from this version once it has been copyedited and typeset.
PLEASE CITE THIS ARTICLE AS DOI: 10.1063/5.0291548

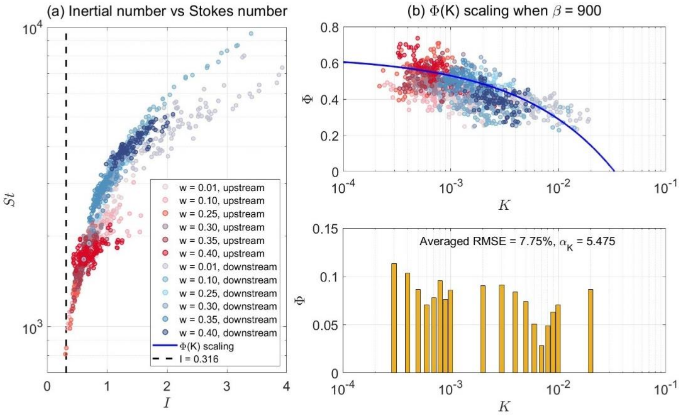

FIG. 11. (a) The relationship between the inertial number, I, and Stokes number, St, for all the tested flows, in which black dash line represents a threshold value of inertial number. (b) Optimal $\Phi(K)$ scaling results when applying $\beta = 900$.

B. Limitations and Future Work

The main limitation of this study lies in not fully exploiting the potential of PTV technique. By tracking the trajectories of individual particles within high-speed images, PTV analysis can describe more complex particle motion (e.g. highly inertial or collisional grain movement under shear) and accurately measure kinematic characteristics that are easily affected by averaging, such as volume fraction cross the depth and granular temperature. In this study, however, PTV is only used to calculate the global solid volume fraction averaged over the entire flow depth, while velocity information and flow depth were derived from PIV analysis, which had been thoroughly validated in previous study. An additional consequence of lacking detailed PTV measurement is that the averaged volume fraction did not exhibit a systematic correlation with basal pore pressure signals, even though local contraction and dilation of granular medium should be among the key factors influencing positive or negative response of basal pore pressures. Future studies could further advance PTV analysis to obtain more detailed solid volume fraction profiles and combine these with velocity profiles, allowing for a more precise characterisation of shear behaviours and local volumetric changes in experimental granular flows. This would be expected to yield deeper insights into the contributions of cohesion or suction in unsaturated flows.

V. CONCLUSIONS

The evolution of solid volume fraction is a key dynamic characteristic of granular flows, governed by dilatancy behaviour, controlled by saturation conditions, and can be predicted using two-phase flow models. However, for unsaturated flows with low water content, simulation of their dilatancy behaviours cannot yet be done with full confidence. This is because recently developed rheological models that account for apparent cohesion effects arising from liquid bridges between solid particles have not been sufficiently supported by empirical data. In this study, we conducted a series of small-scale flume

AIP Publishing
Physics of Fluids
ACCEPTED MANUSCRIPT
This is the author's peer reviewed, accepted manuscript. However, the online version of record will be different from this version once it has been copyedited and typeset.
PLEASE CITE THIS ARTICLE AS DOI: 10.1063/5.0291548

experiments using uniform pseudo-spherical granular materials, with saturation condition varying from fully dry to oversaturated. The temporal and spatial evolution of solid volume fraction was measured utilising Particle Tracking Velocimetry (PTV) techniques. The dilatancy behaviour of the experimental flows was then analysed, and the validity of existing rheological frameworks was evaluated and supported with our experimental data. Here, we conclude our findings as follows:

The rheological behaviours of granular flows exhibit a continuous transition with increasing water content. The experimental flows show consistent evolutionary patterns in flow depth, volume fraction, pore water pressure and thus effective stress. The existence of viscous pore fluid, even at very low water content, can dramatically reduce solid particle collisions which are evident in dry granular flows. After the cohesive effects in unsaturated flows reach the highest level, further increasing water content leads to a gradual increase in pore pressure from negative to positive values, accompanied by a corresponding decrease in effective stress. As a result, the flow mass concentrates towards the flow front with an increased flow depth, while the volume fraction transitions from being relatively stable throughout the flow body to decreasing progressively from flow front to the rear. This corresponds to the distinct fluid effects that depend on the saturation condition. In unsaturated flows, fluid effects are dominated by apparent cohesion, resulting in stronger shear resistance and with lessened dilation; whereas in saturated flows, fluid effects are dominated by viscous drag which reduces intergranular enduring contacts and hence facilitates dilation under shear. This transition in rheological and dilatancy behaviours occurs gradually and continuously with increasing saturation degree.

The $\Phi(I_m)$ scaling law, based on the extended inertial number I_m that accounts for various stress contributions, is shown to successfully predict the dilatancy behaviours of granular flows across both unsaturated and saturated conditions, thereby supporting the validity of the $\mu(I_m)$ and $\Phi(I_m)$ rheological framework over a broader spectrum of flow regime. This represents the first experimental validation of the $\mu(I_m)$ and $\Phi(I_m)$ models. The widely recognised $\Phi(I)$ and $\Phi(K)$ models were initially employed to compare and cross-validate our results for solid volume fraction in dry and wet granular flow experiments. Then, the $\Phi(K)$ model, associated with visco-inertial rheology, and the $\Phi(I_m)$ model, which additionally considers both cohesive and viscous effects of pore fluid, were fitted to the volume fraction data of all the wet granular flows, and the errors from both models were analysed. Under their respective best-fit scenarios, the $\Phi(I_m)$ scaling demonstrates significantly better agreement with the experimental data, spanning from highly unsaturated to oversaturated, than the $\Phi(K)$ scaling. The $\Phi(K)$ model performs well for the prediction of saturated experimental flows as anticipated, but shows clear deviations for that of unsaturated flows. These findings validate the $\mu(I_m)$ rheological framework for two-phase granular flows across a wide range of flow regimes, while highlighting the limitations of the $\mu(K)$ rheology for the same conditions.

AIP Publishing

Physics of Fluids

ACCEPTED MANUSCRIPT

This is the author's peer reviewed, accepted manuscript. However, the online version of record will be different from this version once it has been copyedited and typeset.

PLEASE CITE THIS ARTICLE AS DOI: 10.1063/5.0291548

ACKNOWLEDGEMENTS

The authors acknowledge the financial support from the National Natural Science Foundation of China (Grant No. U24A20618), the Sichuan Science and Technology Program (Grant No. 2024NSFJQ0043), and State Key Laboratory of Hydraulics and Mountain River Engineering, Sichuan University (Grant No. SKHL2308). In addition, we would like to give special thanks to a Leverhulme Trust International Network Grant (#IN-2016-041) awarded to the second author.

DATA AVAILABILITY

The data that supports the findings of this study are available from the corresponding author upon reasonable request.

CONFLICT OF INTEREST

The authors declare that they have no known competing financial interests or personal relationships that could have appeared to influence the work reported in this paper.

AIP Publishing Physics of Fluids ACCEPTED MANUSCRIPT
This is the author's peer reviewed, accepted manuscript. However, the online version of record will be different from this version once it has been copyedited and typeset.
PLEASE CITE THIS ARTICLE AS DOI: 10.1063/5.0291548

REFERENCE

1. Y. Forterre, andO. Pouliquen, *Granular Flows* (Springer Basel, Basel, 2011).

2. L. Sarno, L. Carleo, M. N. Papa, andA. Armanini, "Optical method for measuring the volume fraction of granular media: Application to faced-centered cubic lattices of monodisperse spheres," Physical Review E **101**, 022904 (2020).

3. N. Riley, "Granular Media; Between Fluid and Solid, by Bruno Andreotti, Yoël Forterre and Olivier Pouliquen," Contemporary Physics **55**, 151 (2014).

4. R. M. Iverson, "The physics of debris flows," Reviews of Geophysics **35**, 245 (1997).

5. L. Sarno, M. Nicolina Papa, Y.-C. Tai, L. Carleo, andP. Villani, "A non-invasive stochastic-optical method (SOM) for estimating the volume fraction in granular flows: application on interrogation windows with different aspect ratios," Journal of Physics: Conference Series **1249**, 012013 (2019).

6. F. Chen, andH. Yan, "Constitutive model for solid-like, liquid-like, and gas-like phases of granular media and their numerical implementation," Powder Technology **390**, 369 (2021).

7. Y. Forterre, andO. Pouliquen, "Flows of Dense Granular Media," Annual Review of Fluid Mechanics **40**, 1 (2008).

8. K. Roscoe, A. Schofield, andC. Wroth, "On The Yielding of Soils," Geotechnique **8**, 22 (1958).

9. A. Schofield, andC. Wroth, *Critical State Soil Mechanics* (1968).

10. I. Srivastava, L. E. Silbert, G. S. Grest, andJ. B. Lechman, "Viscometric flow of dense granular materials under controlled pressure and shear stress," Journal of Fluid Mechanics **907**, A18 (2021).

11. F. Bouchut, E. Drach, E. D. Fernández-Nieto, A. Mangeney, andG. Narbona-Reina, "A series of two-phase models for grain–fluid flows with dilatancy," Journal of Fluid Mechanics **1008**, A43 (2025).

12. R. M. Iverson, M. Logan, R. G. LaHusen, andM. Berti, "The perfect debris flow? Aggregated results from 28 large-scale experiments," Journal of Geophysical Research: Earth Surface **115**, (2010).

13. L. Rondon, O. Pouliquen, andP. Aussillous, "Granular collapse in a fluid: Role of the initial volume fraction," Physics of Fluids **23**, 73301 (2011).

14. N. Andreini, C. Ancey, andG. Epely-Chauvin, "Granular suspension avalanches. II. Plastic regime," Physics of Fluids **25**, (2013).

15. R. M. Iverson, andD. L. George, "Modelling landslide liquefaction, mobility bifurcation and the dynamics of the 2014 Oso disaster," Géotechnique **66**, 175 (2016).

ACCEPTED MANUSCRIPT
Physics of Fluids
AIP Publishing
This is the author's peer reviewed, accepted manuscript. However, the online version of record will be different from this version once it has been copyedited and typeset.
PLEASE CITE THIS ARTICLE AS DOI: 10.1063/5.0291548

16. G. T. Houlsby, *How the dilatancy of soils affects their behaviour* (Florence, Italy, 1991).

17. O. Cinicioglu, A. Abadkon, A. Altunbas, andM. Abzal, *Variation of friction angle and dilatancy for anisotropic cohesionless soils* (2013).

18. M. Bandi, P. Das, O. Gendelman, H. George, H. Hentschel, andI. Procaccia, "Universal Scaling Laws for Shear Induced Dilation in Frictional Granular Media," Granular Matter **21**, 40 (2019).

19. A. A. Ouici, T. A. Cherif, M. Youcef, andM. and Belkhatir, "Influence of fines and gravel particles on strength-dilatancy of river sand: Effect of depositional conditions," Marine Georesources & Geotechnology 1 (2024).

20. Z.-L. Dong, C.-X. Tong, S. Zhang, Y. P. Cheng, andD. Sheng, "Strength and dilatancy of crushable soils with different gradings," Canadian Geotechnical Journal **62**, 1 (2025).

21. O. Pouliquen, C. Cassar, P. Jop, Y. Forterre, andM. Nicolas, "Flow of dense granular material: towards simple constitutive laws," Journal of Statistical Mechanics: Theory and Experiment **2006**, P07020 (2006).

22. K. F. E. Cui, G. G. D. Zhou, andL. Jing, "Viscous Effects on the Particle Size Segregation in Geophysical Mass Flows: Insights From Immersed Granular Shear Flow Simulations," Journal of Geophysical Research: Solid Earth **126**, e2021JB022274 (2021).

23. Y. Ren, F. Cai, Q. Yang, andZ. Su, "Contact-dependent inertial number and μ(I) rheology for dry rock-ice granular materials," Engineering Geology **350**, 107995 (2025).

24. G. D. R. MiDi, "On dense granular flows," The European Physical Journal E **14**, 341 (2004).

25. D. G. Schaeffer, T. Barker, D. Tsuji, P. Gremaud, M. Shearer, andJ. M. N. T. Gray, "Constitutive relations for compressible granular flow in the inertial regime," Journal of Fluid Mechanics **874**, 926 (2019).

26. A. Lemaître, J.-N. Roux, andF. Chevoir, "What do dry granular flows tell us about dense non-Brownian suspension rheology?," Rheologica Acta **48**, 925 (2009).

27. J. F. Brady, andG. Bossis, "Stokesian Dynamics," Annual Review of Fluid Mechanics **20**, 111 (1988).

28. S. Siman-Tov, andE. E. Brodsky, "Distinguishing between rheophysical regimes of fluid-saturated granular-flows using dilatancy and acoustic emission measurements," Granular Matter **23**, 44 (2021).

29. C. Cassar, M. Nicolas, andO. Pouliquen, "Submarine granular flows down inclined planes," Physics of Fluids **17**, (2005).

30. F. Boyer, É. Guazzelli, andO. Pouliquen, "Unifying Suspension and Granular

ACCEPTED MANUSCRIPT
Physics of Fluids
AIP Publishing
This is the author's peer reviewed, accepted manuscript. However, the online version of record will be different from this version once it has been copyedited and typeset.
PLEASE CITE THIS ARTICLE AS DOI: 10.1063/5.0291548

Rheology," Physical Review Letters **107**, 188301 (2011).

31. A. Pellegrino, L. Schippa, O. Pouliquen, andE. Guazzelli, *Experiments in shear flow of granular-fluid suspension and dense mixture* (2014).

32. M. Trulsson, B. Andreotti, andP. Claudin, "Transition from the Viscous to Inertial Regime in Dense Suspensions," Physical Review Letters **109**, (2012).

33. R. M. Iverson, "Regulation of landslide motion by dilatancy and pore pressure feedback," Journal of Geophysical Research **110**, (2005).

34. R. Iverson, andD. George, "A depth-averaged debris-flow model that includes the effects of evolving dilatancy. I. Physical basis," Proceedings of the Royal Society A: Mathematical, Physical and Engineering Sciences **470**, 20130819 (2014).

35. R. M. Iverson, "Scaling and design of landslide and debris-flow experiments," Geomorphology **244**, 9 (2015).

36. D. George, andR. Iverson, "A depth-averaged debris-flow model that includes the effects of evolving dilatancy. II. Numerical predictions and experimental tests," Proceedings of the Royal Society A: Mathematical, Physical and Engineering Sciences **470**, 20130820 (2014).

37. F. Bouchut, E. D. Fernández-Nieto, A. Mangeney, andG. Narbona-Reina, "A two-phase two-layer model for fluidized granular flows with dilatancy effects," Journal of Fluid Mechanics **801**, 166 (2016).

38. M. Rauter, "The compressible granular collapse in a fluid as a continuum: validity of a Navier–Stokes model with $\mu (J)$, $\phi (J)$-rheology," Journal of Fluid Mechanics **915**, A87 (2021).

39. X. Meng, Y. Wang, C. Wang, andJ.-T. Fischer, "Modeling of unsaturated granular flows by a two-layer approach," Acta Geotechnica **12**, 677 (2017).

40. M. Scheel, R. Seemann, M. Brinkmann, M. Di Michiel, A. Sheppard, andS. Herminghaus, "Liquid distribution and cohesion in wet granular assemblies beyond the capillary bridge regime," Journal of Physics: Condensed Matter **20**, 494236 (2008).

41. R. S. Sharma, andA. Sauret, "Experimental models for cohesive granular materials: a review," Soft Matter **21**, 2193 (2025).

42. D. Fredlund, andH. Rahardjo, *Soil Mechanics for Unsatured Soils* (1993).

43. A. Alnmr, M. O. Alzawi, R. Ray, S. Abdullah, andJ. Ibraheem, "Experimental Investigation of the Soil-Water Characteristic Curves (SWCC) of Expansive Soil: Effects of Sand Content, Initial Saturation, and Initial Dry Unit Weight," Water **16**, 627 (2024).

44. G. G. D. Zhou, N. G. Wright, Q. Sun, andQ. Cai, "Experimental Study on the Mobility of Channelized Granular Mass Flow," Acta Geologica Sinica - English Edition **90**, 988 (2016).

AIP Publishing
Physics of Fluids
ACCEPTED MANUSCRIPT
This is the author's peer reviewed, accepted manuscript. However, the online version of record will be different from this version once it has been copyedited and typeset.
PLEASE CITE THIS ARTICLE AS DOI: 10.1063/5.0291548

45. Y. Zhao, W. A. Take, R. Kaitna, B. W. McArdell, J. N. McElwaine, andE. T. Bowman, "Fluid effects in model granular flows," Granular Matter **26**, 2 (2023).

46. M. Badetti, A. Fall, D. Hautemayou, F. Chevoir, P. Aimedieu, S. Rodts, andJ.-N. Roux, "Rheology and microstructure of unsaturated wet granular materials: Experiments and simulations," Journal of Rheology **62**, 1175 (2018).

47. P. S. Raux, andA.-L. Biance, "Cohesion and agglomeration of wet powders," Physical Review Fluids **3**, 014301 (2018).

48. T. T. Vo, S. Nezamabadi, P. Mutabaruka, J.-Y. Delenne, andF. Radjai, "Additive rheology of complex granular flows," Nature Communications **11**, 1476 (2020).

49. S. Coombs, "A physical investigation of the flow structure and mobility behaviour of collisional granular landslides," 2018.

50. A. M. Taylor-Noonan, E. T. Bowman, B. W. McArdell, R. Kaitna, J. N. McElwaine, andW. A. Take, "Influence of Pore Fluid on Grain-Scale Interactions and Mobility of Granular Flows of Differing Volume," Journal of Geophysical Research: Earth Surface **127**, e2022JF006622 (2022).

51. W. Brevis, Y. Niño, andG. Jirka, "Integrating cross-correlation and relaxation algorithms for particle tracking velocimetry," Experiments in Fluids **50**, 135 (2011).

52. F. Tauro, R. Piscopia, andS. Grimaldi, "Streamflow Observations From Cameras: Large-Scale Particle Image Velocimetry or Particle Tracking Velocimetry?," Water Resources Research **53**, 10374 (2017).

53. A. M. Gomez, M. Nikku, S. Shah, D. V. Gradov, andP. Jalali, "Collisional forces and flow characteristics of a stream of falling particles in interaction with a large stationary sphere," Powder Technology **421**, 118447 (2023).

54. D. Gollin, W. Brevis, E. T. Bowman, andP. Shepley, "Performance of PIV and PTV for granular flow measurements," Granular Matter **19**, 42 (2017).

55. S. B. Savage, andK. Hutter, "The motion of a finite mass of granular material down a rough incline," Journal of Fluid Mechanics **199**, 177 (1989).

56. F. Bettella, T. Bisantino, V. D'Agostino, andF. Gentile, *Debris-flow runout distance: Laboratory experiments on the role of Bagnold, Savage and friction numbers* (2012).

57. T. de Haas, A. S. Åberg, F. Walter, andZ. Zhang, "Deciphering seismic and normal-force fluctuation signatures of debris flows: An experimental assessment of effects of flow composition and dynamics," Earth Surface Processes and Landforms **46**, 2195 (2021).

58. G. Zhou, S. li, D. Song, C. Choi, andX. Chen, "Depositional mechanisms and morphology of debris flow: physical modelling," Landslides **16**, 1 (2018).

59. M. Berti, R. Genevois, A. Simoni, andP. R. Tecca, "Field observations of a debris flow event in the Dolomites," Geomorphology **29**, 265 (1999).

Physics of Fluids ACCEPTED MANUSCRIPT
AIP Publishing
This is the author's peer reviewed, accepted manuscript. However, the online version of record will be different from this version once it has been copyedited and typeset.
PLEASE CITE THIS ARTICLE AS DOI: 10.1063/5.0291548

60. S. W. McCoy, G. E. Tucker, J. W. Kean, andJ. A. Coe, "Field measurement of basal forces generated by erosive debris flows," Journal of Geophysical Research: Earth Surface **118**, 589 (2013).

61. J. A. Coe, D. A. Kinner, andJ. W. Godt, "Initiation conditions for debris flows generated by runoff at Chalk Cliffs, central Colorado," Geomorphology **96**, 270 (2008).

62. H.-T. Chou, Y.-L. Chang, andS.-C. Zhang, "Acoustic signals and geophone response of rainfall-induced debris flows," Journal of the Chinese Institute of Engineers **36**, 335 (2013).

63. G. L. Bennett, P. Molnar, B. W. McArdell, andP. Burlando, "A probabilistic sediment cascade model of sediment transfer in the Illgraben," Water Resources Research **50**, 1225 (2014).

64. C. Berger, B. W. McArdell, andF. Schlunegger, "Direct measurement of channel erosion by debris flows, Illgraben, Switzerland," Journal of Geophysical Research: Earth Surface **116**, (2011).

65. A. Badoux, C. Graf, J. Rhyner, R. Kuntner, andB. W. McArdell, "A debris-flow alarm system for the Alpine Illgraben catchment: design and performance," Natural Hazards **49**, 517 (2009).

66. L. Marchi, M. Arattano, andA. M. Deganutti, "Ten years of debris-flow monitoring in the Moscardo Torrent (Italian Alps)," Geomorphology **46**, 1 (2002).

67. T. Takahashi, *Debris flow : mechanics, prediction and countermeasures* (Taylor & Francis, London ;, 2007).

68. H. Suwa, K. Okano, andT. Kanno, "Behavior of debris flows monitored on test slopes of Kamikamihorizawa Creek, Mount Yakedake, Japan," International Journal of Erosion Control Engineering **2**, 33 (2009).

69. K. Okano, H. Suwa, andT. Kanno, "Characterization of debris flows by rainstorm condition at a torrent on the Mount Yakedake volcano, Japan," Geomorphology **136**, 88 (2012).

70. N. Sanvitale, andE. T. Bowman, "Visualization of dominant stress-transfer mechanisms in experimental debris flows of different particle-size distribution," Canadian Geotechnical Journal **54**, 258 (2017).

71. X. Meng, A. Taylor-Noonan, C. Johnson, W. Take, E. Bowman, andJ. Gray, "Granular-fluid avalanches: the role of vertical structure and velocity shear," Journal of Fluid Mechanics **980**, A11 (2024).

72. E. Bowman, R. Kaitna, B. McArdell, J. McElwaine, N. Sanvitale, W. A. Take, A. Taylor-Noonan, andY. Zhao, *The Rosetta Stone Project – Integrating experimental results on debris flow mechanics across the scales: first results* (2021).

73. E. Bowman, A. Fawley, R. Kaitna, S. li, B. McArdell, J. McElwaine, N. Sanvitale, W. Take, L. Tauskela, A. Taylor-Noonan, andY. Zhao, "The Rosetta Stone Project –

ACCEPTED MANUSCRIPT
Physics of Fluids
AIP Publishing
This is the author's peer reviewed, accepted manuscript. However, the online version of record will be different from this version once it has been copyedited and typeset.
PLEASE CITE THIS ARTICLE AS DOI: 10.1063/5.0291548

Integrating experimental results on debris flow mechanics across the scales: Next results," E3S Web of Conferences **415**, (2023).

74. T. Börzsönyi, andR. E. Ecke, "Rapid granular flows on a rough incline: Phase diagram, gas transition, and effects of air drag," Physical Review E **74**, 061301 (2006).

75. K. Kelfoun, "A two-layer depth-averaged model for both the dilute and the concentrated parts of pyroclastic currents," Journal of Geophysical Research: Solid Earth **122**, 4293 (2017).

76. D. Huang, G. Sun, andK. Lu, "Influence of granule velocity on gravity-driven granular flow," Physics Letters A **375**, 3375 (2011).

77. O. Reynolds, "LVII. On the dilatancy of media composed of rigid particles in contact. With experimental illustrations," The London, Edinburgh, and Dublin Philosophical Magazine and Journal of Science **20**, 469 (1885).

78. Y.-R. Chen, andB. Kutter, "Contraction, Dilation, and Failure of Sand in Triaxial, Torsional, and Rotational Shear Tests," Journal of Engineering Mechanics-ASCE **135**, 1155 (2009).

79. R. A. Bagnold, "Experiments on a gravity-free dispersion of large solid spheres in a Newtonian fluid under shear," Proceedings of the Royal Society of London. Series A **225**, 49 (1954).

80. S. Taylor, andE. Brodsky, "Granular temperature measured experimentally in a shear flow by acoustic energy," Physical Review E **96**, (2017).

81. F. Tapia, M. Ichihara, O. Pouliquen, andÉ. Guazzelli, "Viscous to Inertial Transition in Dense Granular Suspension," Physical Review Letters **129**, 078001 (2022).

82. L. Amarsid, J. Y. Delenne, P. Mutabaruka, Y. Monerie, F. Perales, andF. Radjai, "Viscoinertial regime of immersed granular flows," Physical Review E **96**, 012901 (2017).

83. K. F. E. Cui, G. G. D. Zhou, L. Jing, X. Chen, andD. Song, "Generalized friction and dilatancy laws for immersed granular flows consisting of large and small particles," Physics of Fluids **32**, (2020).

84. Y. Xie, G. G. D. Zhou, K. F. E. Cui, andX. Lu, "Numerical investigation of debris flows using a two-phase continuum model incorporating a visco-inertial rheology," Engineering Geology **308**, 106797 (2022).

85. C. Ness, andJ. Sun, "Flow regime transitions in dense non-Brownian suspensions: Rheology, microstructural characterization, and constitutive modeling," Physical Review E **91**, 012201 (2015).

86. S. B. Savage, *The Mechanics of Rapid Granular Flows* (Elsevier, 1984).